ACS OMEGA

http://pubs.acs.org/journal/acsodf

Article

Long-Lived Afterglow from Elemental Sulfur Powder: Synergistic Effects of Impurity and Structure

Jiaqi Guo,[#] Zhangdi Lu,[#] Chenmin Li, Yuming Miao, Bingbing Zhang, Jacky W. Y. Lam, Yu-e Shi,* Zhenguang Wang,* and Ben Zhong Tang*

Cite This: *ACS Omega* 2022, 7, 30582−30589

Read Online

ACCESS | Metrics & More | Article Recommendations | Supporting Information

ABSTRACT: Elemental sulfur is not traditionally considered as an afterglow material, even though it can be endowed with fluorescence properties through processing it into nanodots. Herein, we discovered that elemental sulfur powder could emit room temperature phosphorescence (RTP) with a lifetime of 3.7 ms. A long-lived (>12 s) afterglow emission at 77 K could also be observed by the naked eye. Detailed investigations suggested that such a special phenomenon was attributed to impurity-related traps coupled with conduction and valence bands. After the sulfur is processed into nanodots, the rigid environment formed by the cross-linking of the surface ligands could stabilize the excited charges from quenching. This results in the promotion of RTP intensity and lifetime to achieve an emission lifetime of 200 ms. These results confirm the unique RTP of elemental sulfur powder, and also suggest the potential of sulfur-based materials as versatile components for the development of RTP materials.

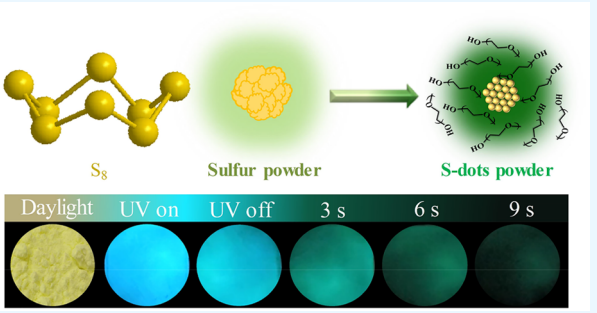

INTRODUCTION

Room temperature phosphorescence (RTP) materials play important roles in various fields such as bioimaging, anticounterfeiting, and warning signs, because of their features of high signal-to-background ratio and long emission lifetime, involving triplet states and large Stokes shifts.[1−6] Some traditional RTP materials, with excellent photophysical properties, have been reported, including transition metal-based complexes, rare-earth doped phosphors, and pure organic molecules or composites.[5,7−9] However, these RTP materials still suffer from several disadvantages: (a) expensive or/and highly toxic raw materials; (b) complicated and high energy consumption production processes; (c) stringent conditions are required for effectively generating afterglow emissions, such as the bulk form for rare-earth-based materials and the crystalline states for pure organic compounds.[10−13] These disadvantages significantly hindered their wider applications, which also forced researchers to develop alternative RTP materials, with superior photophysical properties, synthesized through facile preparation strategies, utilizing inexpensive and nontoxic raw materials. Among them, efforts have been made to modulate the RTP of nanomaterials, produced by wet chemical synthesis under mild conditions, and these efforts have recently been extended toward the inexpensive and easily accessible pure elemental materials, such as carbon, silicon, and sulfur.[14−18] Many carbon-based RTP materials have been reported, and several strategies were proposed to generate and promote their RTP performances.[19−22] It is noted that matrices have been usually used to immobilize the luminophores, aiming to stabilize the triplet state and make the effective radiative transition possible through the spin-forbidden process.

Elemental sulfur is a type of earth-abundant natural mineral, which is also a massive byproduct of the petrochemical industry.[23,24] Compared with other commonly used RTP materials, elemental sulfur offers unique antimicrobial properties, is involuntarily produced and earth-abundant, and possesses inherent antimicrobial features.[25−27] Thus, there is a rather strong drive to utilize elemental sulfur for developing RTP materials. Elemental sulfur has been reported to show dim fluorescence for a long time, due to the direct band-to-band radiative recombination between excited electrons and holes.[28,29] Emission efficiency can be significantly improved after processing it into nanosized sulfur nanodots (S-dots). For example, Shen and co-workers reported that processing the elemental sulfur powder into S-dots resulted in an obvious improvement of photoluminescence (PL) quantum yield (QY) of 3.8%.[30] Our group also reported the H_2O_2-assisted strategy to produce highly emissive S-dots, achieving a PL QY of

Received: July 8, 2022
Accepted: August 12, 2022
Published: August 20, 2022

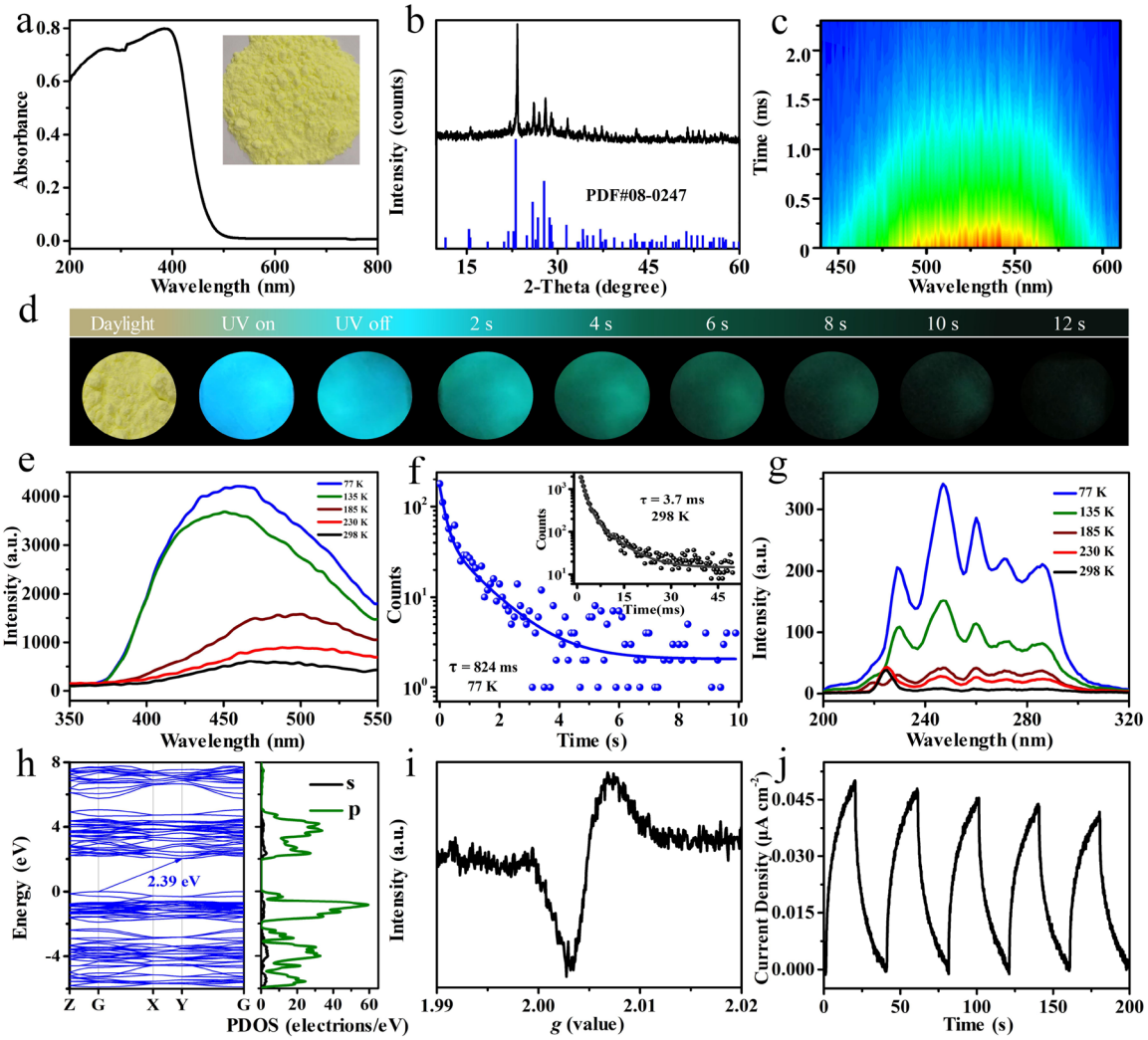

Figure 1. Characterizations of elemental sulfur powder. (a) UV−visible absorption spectrum, with its photograph showing as inset; (b) XRD pattern; (c) time-resolved emission scanning spectrum under the excitation of 280 nm; (d) digital photos before and after switching off 254 nm UV light at 77 K; (e) temperature-dependent phosphorescence spectra, (f) emission lifetime, and (g) phosphorescence excitation spectra; (h) calculated (left) electronic band structures and (right) densities of states (DOS); (i) EPR spectrum; (j) evolution of current density as a function of irradiation time with a xenon lamp.

23%.[31] Zhou and co-workers reported that the emission color and PL QY can be modulated by controlling the oxygen content of the reaction system.[32] However, RTP properties have never been reported in S-dots, let alone with the powder of elemental sulfur powder.

In this work, we report that the powder of elemental sulfur shows dim RTP in the blue-to-green region with an emission lifetime up to 3.7 ms. After theoretical and experimental investigations, the impurity-related traps coupled with conduction and valence bands were identified as the origin of the RTP emission. The intensity of the RTP emission could be obviously prompted after processing the sulfur powder into nanodots, and an emission lifetime of 200 ms was detected at room temperature. Benefiting from the rigid environment formed by the ligands on the surface of S-dots, afterglow emission was recorded at room temperature, which enabled the triple lifetime-encoding for information encryption.

RESULTS AND DISCUSSION

Elemental sulfur powder is amber-colored (Figure 1a inset), showing intrinsic semiconductor-like absorption in the wavelength range from 200 to 450 nm.[33] Its band gap is 2.79 eV, determined from Figure 1a. Figure 1b gives the X-ray diffraction (XRD) pattern of elemental sulfur powder studied here, which matches with the sulfur references of PDF#08-0247.[28,34] Surprisingly, elemental sulfur exhibits RTP emission in the blue-to-green region (Figure 1c). The RTP emission is rather weak, which could not be observed by a camera and naked eyes at room temperature (Figure S1). After decreasing the temperature to 77 K, elemental sulfur powder shows intensive cyan emission under the irradiation of 254 nm UV light. After switching off the excitation light, the emission color changes to green, and the afterglow emission could be observed even for nearly 12 s (Figure 1d, Video S1). To get more insight into the origins of RTP emission from elemental sulfur powder, temperature-dependent phosphorescence emission/excitation spectra and lifetime measurements were conducted. There are minor differences in the RTP spectra recorded by steady-state spectra and time-resolved emission spectra measurements due to the difference in the detection model. A promoted phosphorescence intensity (Figure 1e) and extended lifetime (Figure 1f and Table S1, from 3.7 to 824 ms)

https://doi.org/10.1021/acsomega.2c04307
ACS Omega 2022, 7, 30582−30589

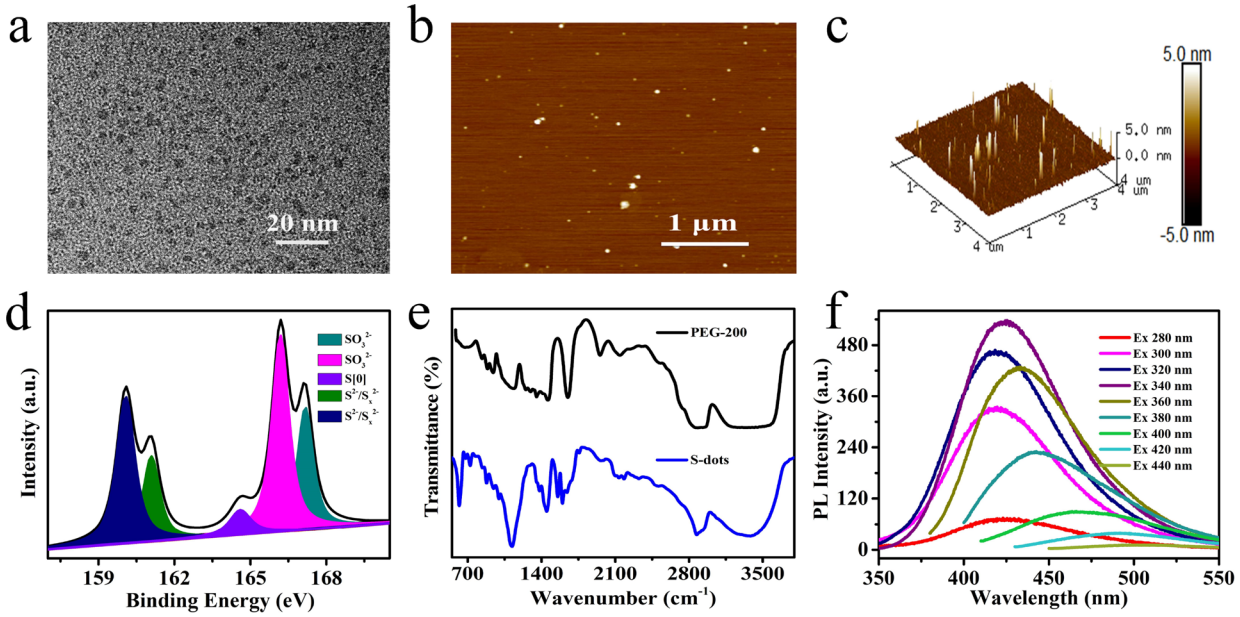

Figure 2. Characterizations of S-dots. (a) TEM, (b, c) AFM images, (d) XPS S_{2p}, (e) FTIR, and (f) photoluminescence spectra excited under different wavelength.

can be observed alongside the decreasing detection temperature from 298 to 77 K. This ruled out the possibility of a thermally activated delayed fluorescence mechanism. With the decrease of detection temperature, relatively broad spectra and a blue shift on the peak maximum are observed. This suggests the presence of multiple emission centers, causing the diversity of impurity-related traps in elemental sulfur powder. We also collected the temperature-dependent phosphorescence spectra at different excitation wavelengths. As shown in Figure S2a-2e, the phosphorescence intensity varies with the evolution of excitation wavelengths. While, the shape and peak maximum of spectra are almost identical under different excitation wavelengths. The intensity of phosphorescence excitation also increases with the decreasing detection temperature (Figure 1g). The excitation spectra present a relatively wide peak in the range from 220 to 300 nm, which matches well with the absorption spectrum of elemental sulfur in the UV range (Figure 1a). This suggests the close relationship between the RTP emission and the electronic structure of elemental sulfur. In addition, relatively broad spectra with a blue shift of the peak maximum are observed with the decrease of detection temperature. This suggests the presence of multiple emission centers. To understand the electronic structure of elemental sulfur, density functional theory (DFT) calculations were conducted. Figure 1h shows the simulated band structure of elemental sulfur, showing a direct band gap of 2.39 eV, which is 0.4 eV smaller than the determined value (2.79 eV). This can be explained by the well-known band gap underestimation within the framework of standard DFT.[28] The conduction and valence bands are attributed to the major sulfur p orbitals and s orbitals. The presence of a wide valence band is also confirmed by the X-ray photoelectron spectroscopy (XPS) valence band spectrum (Figure S3).[28]

Electron paramagnetic resonance (EPR) spectroscopy was used to explore the interaction between electromagnetic radiation and magnetic moments of charges.[35] A strong signal at g = 2.0048 can be observed on the EPR spectrum (Figure 1i), suggesting the presence of trapped holes in elemental sulfur.[36] This is further confirmed by the photoconductivity curves of elemental sulfur, which show an obvious increase in the current density under the irradiation of light (Figure 1j). Thus, we conclude that the RTP emission originates from the charge carrier traps in the elemental sulfur, which recombines with the conduction and valence bands. The presence of lattice defects can be excluded, suggested by the identical phosphorescence properties of elemental sulfur with different crystalline forms. Traps induced by incorporating impurities are one of the widely accepted mechanisms for RTP emission in classical inorganic systems.[10,17,36] Inspired by this mechanism, the composition of elemental sulfur powder was examined by ICP-OES, showing the presence of a trace amount of Si, Ca, and P (Table S2). Thus, we proposed that the RTP emission originated from the impurity-related traps coupled with conduction and valence bands. To support our hypothesis, the photophysical properties of sulfur powder with different purities were studied. The afterglow of sulfur powder is rather weak, and it is difficult to compare the intensity or peak position of the emission spectra. Thus, we studied the phosphorescence spectra of sulfur powder with different purities, at 77 K. As shown in Figure S4, almost identical phosphorescence spectra were recorded on the elemental sulfur powder before and after purification at 77 K. However, the phosphorescence intensity significantly decreased after the purification process (Figure S4a,b). This suggests the contribution of the impurity to the phosphorescence of elemental sulfur, and purification results in the decrease of impurity-related traps. Combining the results of EPR, DFT calculations, and photoconductivity curves, we conclude that the afterglow originates from the impurity-related traps coupled with conduction and valence bands. This is further confirmed by the phosphorescence spectra of elemental sulfur with higher purity (99.99%), where identical spectra and decreased intensity were observed compared with that elemental sulfur with a purity of 99.9% (Figure S4c). We failed to identify the accurate composition of impurities, as it was difficult to purify and extract the impurities from the sulfur

https://doi.org/10.1021/acsomega.2c04307
ACS Omega 2022, 7, 30582−30589

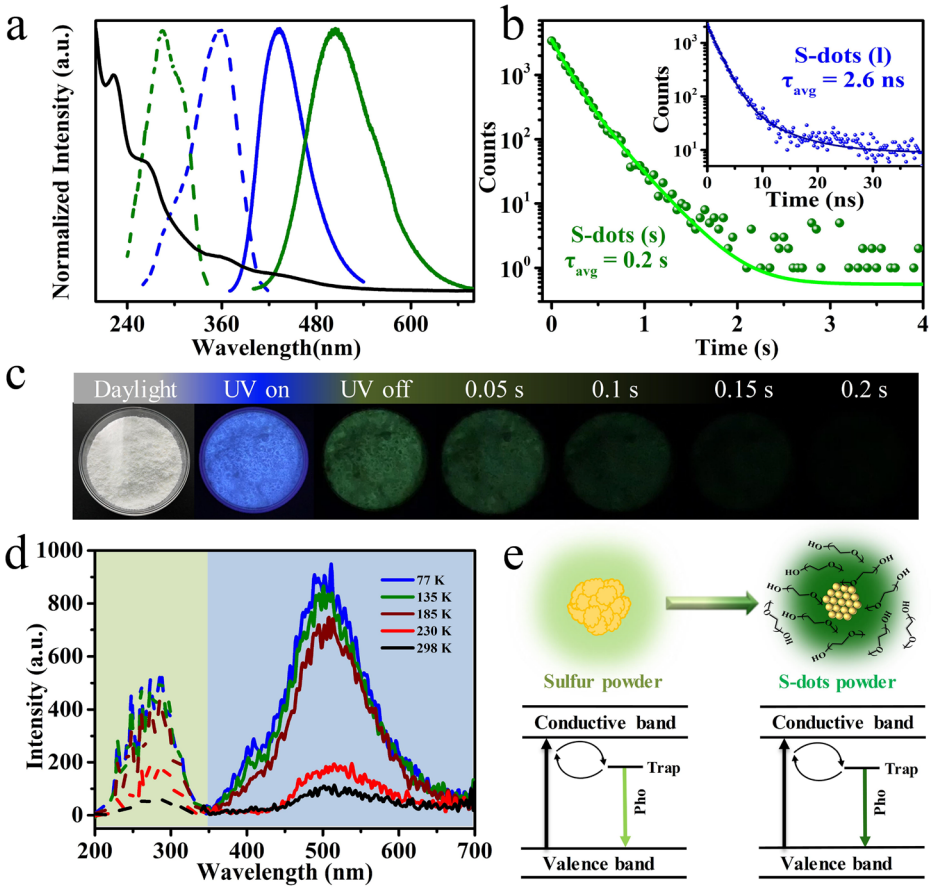

Figure 3. (a) Steady-state PL/excitation (blue line, excited at 340 nm) and phosphorescence/excitation (green line, excited at 280 nm) spectra, and the UV−visible absorption spectra of S-dots powder; (b) emission decay curves of S-dots in solution (blue line) and powder states (green line), excited at 280 nm; (c) digital photos of S-dots powder before and after switching off 302 nm UV light at room temperature; (d) temperature-dependent phosphorescence (solid line) and excitation (dashed line) spectra of S-dots powder; (e) schematic illustration of the RTP mechanism of sulfur powder and S-dots.

powder with a purity of 99.9%. We conducted the purification of elemental sulfur powder through recrystallization and sublimation. However, differences in XPS (Figure S5), XRD (Figure S6), and photoconductivity measurements (Figure S7) can be observed between the purified sulfur samples and the raw materials.

To further promote the RTP intensity of elemental sulfur power, S-dots were synthesized by an H_2O_2-assisted top-down method, under the passivation of polyethylene glycol (PEG). Intensive blue emission can be observed on the solution of S-dots under the irradiation of UV light. The formation of S-dots was confirmed by the results of TEM (Figure 2a) and AFM (Figure 2b,c) imaging. After the etching by H_2O_2, monodispersed S-dots with a size as small as about 5 nm were obtained. In addition, the full scan XPS spectrum shows that the S-dots are composed of C, O, and S (Figure S8a). Then, energy dispersive spectroscopy was used to study the content of each element. As shown in Figure S8b, S-dots were composed of C, O, Na, and S, with a content of 32.9, 26.6, 24.0, and 16.5%, respectively. The valence states of S were studied by analyzing the high-resolution spectrum of S_{2p}, which could be fitted into five peaks. As shown in Figure 2d, the peaks at 160.1 and 161.1 eV, corresponding to S^{2-} and polysulfide (S_x^{2-}), suggest the etching of elemental sulfur by NaOH.[30] The intensive peak at 164.6 eV suggests the presence of atomic sulfur, while the peaks at 166.2 and 167.2 eV are attributed to SO_3^{2-} ($2p_{3/2}$) and SO_3^{2-} ($2p_{1/2}$), respectively.[32] This suggests that S-dots are composed of central elemental sulfur, coated with sulfonate groups, divalent sulfur ions, and PEG. FTIR spectra were further recorded to study the states of PEG on the surface of S-dots. Compared with that of pure PEG, an almost identical spectrum was observed for S-dots, and no new peaks can be recognized after forming S-dots. This suggests PEG is physically absorbed on the surface of S-dots, without any chemical reactions.

The solution of S-dots shows intensive blue emission, with maximal emission and excitation wavelengths of 432 and 360 nm (Figure S9), respectively. S-dots show excitation-dependent emission properties (Figure 2f), which are further evaluated by comparing the emission peak maximums and relative intensities under different excitation wavelengths (Figure S10).[19,20] In the excitation wavelength range from 280 to 330 nm, with the increase of excitation wavelength, a sharp increase in the emission intensities is observed with almost identical emission peak maximums (420 nm). Shifting the excitation wavelength to a longer range leads to the PL peak redshift from 450 to 560 nm, quickly dropping the PL intensity to zero at the excitation wavelength beyond 450 nm. These results are consistent with previous works, demonstrating the multiple emission species in the S-dot sample.[30,32]

The solid powder can be obtained through freeze-drying treatment of the solution of S-dots, which also shows strong

https://doi.org/10.1021/acsomega.2c04307
ACS Omega 2022, 7, 30582−30589

blue emission, with maximal emission and excitation wavelengths of 425 and 340 nm (Figure 3a), respectively. They also show excitation-dependent emission properties, presenting similar evolution trends with a function of excitation wavelength with that of S-dots in solution (Figure S11). The excitation-dependent PL QY was also recorded on the S-dots powder (Table S3). This suggests the freeze-drying treatment did not lead to the decomposition of S-dots and varying emission species. UV−vis absorption spectra of the powder demonstrate that S-dots present obvious peaks located at 220, 265, 370, and 450 nm (Figure 3a). The obvious peak at 220 nm can be attributed to the n → σ^* transition of nonbonding electrons of S.[37] The peaks at 265 and 370 nm indicate the presence of S_2^{2-} and S_8^{2-}.[38] The peak at 450 nm is related to the bandgap transitions of elemental sulfur, with a band gap of 2.79 eV, showing intrinsic semiconductor-like properties.[28] As expected, the powder shows RTP properties (Video S2). The peak maximum of the phosphorescence spectrum locates in the green region (Figure 3a), which almost keeps constant with various excitation wavelengths (Figure S12). The excitation-independent RTP properties are quite different from the excitation-dependent fluorescence properties, suggesting a totally different origin of emission. This is further confirmed by the significant promotion of the emission lifetime (from 2.6 ns to 0.2 s) of S-dots, after processing them from aqueous solution to solid (Figure 3b, Table S4). After processing into S-dots, the afterglow intensity was greatly enhanced, which allowed us to record the afterglow images at room temperature. After switching off UV light, a green afterglow is observed, and this is also consistent with the phosphorescence emission spectra of S-dots. Note that the emission color and duration in Figure 3c are different from that shown in Figure 1d, which is mainly caused by the different detection temperatures.

By decreasing the detection temperature from 298 to 77 K, phosphorescence emission/excitation intensities were enhanced by 9-fold (Figure 3d) and emission lifetime was extended (0.2 to 1.0 s, Figure S13 and Table S5) without shifting the peak maximums. There is no shift in the peak maximum when changing detection temperature from 77 to 298 K. This suggests that processing sulfur powder into S-dots has eliminated certain types of impurity-related traps, and only green emission-related traps are reserved. This is also consistent with the process of producing S-dots, which involves the dispersion and etching of elemental sulfur powder in NaOH solution, flowed by the dialysis process. During this process, some impurities may be dissolved and excluded in the final products of S-dots powder. We also compared the phosphorescence excitation spectra of both elemental sulfur powder and S-dots powder at different temperatures. As presented in Figure S14, almost identical spectra were obtained. Note that the peak on the spectra of elemental sulfur powder is relatively broad, caused by a weak emission in nature. This suggests that the RTP of the S-dots originates from the impurity-related traps coupled with conduction and valence bands in elemental sulfur powder, and processing the powder into nanodots has greatly promoted their RTP intensities. Our hypothesis was further confirmed by EPR and photoconductivity measurements, which present the strong signal of charge carriers (Figure S15) and increased current density under the irradiation of light (Figure S16), respectively.

The origin of RTP emission was further studied by comparing the optical properties of products obtained by various control experiments. No fluorescence and RTP can be observed on the products obtained through control experiments without adding elemental sulfur and PEG (data not shown), suggesting the significant roles of both the atomic sulfur core and surface ligands on the luminescence of S-dots. In addition, no RTP can be recorded on the products obtained by the reaction between PEG with different molecular weights and NaOH under different conditions, including heating, ultrasonication, and hydrothermal treatment (data not shown), which excludes the bias results from forming cross-linked polymers or carbon dots by PEG. The effects of the amount and molecular weight of PEG on the RTP performances of S-dots were systematically studied. As shown in Figures S17 and S18, no change on the peak maximum can be observed when varying the amount and molecular weight of PEG. The highest phosphorescence intensity is achieved by adding 3 mL of PEG and selecting PEG-200 as the ligands. Injection of H_2O_2 into the reaction system is also essential for achieving high-performance RTP (Figure S19). Without the addition of H_2O_2, the obtained products are viscous, which is difficult to produce into a powder due to the relatively high water-absorbing ability of the products. Changing these synthesis conditions has no obvious effects on the emission lifetime of S-dots powder (Table S6−S8), which suggests that the same emission center is produced under these conditions. Based on the above observations, we conclude that the RTP of S-dots originates from the impurity-related traps coupled with conduction and valence bands in elemental sulfur powder, and processing them into nanodots can promote the intensities of emission, benefiting from the rigid environment formed by the cross-linking of PEG (Figure 3e). The rigid environment could stabilize the excited charges from quenching by the environment, such as oxygen, solvents, and nonradiative transitions.

Given the afterglow emission properties of elemental sulfur and S-dots, their potential applications in information encryption were demonstrated. The full flower with white and blue emissions can be observed under daylight and UV light, respectively. Only the very center of the flower can be observed, after switching off the UV light (Figure 4). Therefore, triple lifetime-encoding for information encryption is achieved by using products with different lifetimes.

CONCLUSION

We discover that elemental sulfur powder, a massively produced industrial byproduct, holds RTP emission with a lifetime up to 3.7 ms. The RTP emission was attributed to the impurity-related traps coupled with conduction and valence bands in sulfur powder. Particularly, similar yet greatly promoted RTP intensity and lifetime could be observed after processing the sulfur powder into S-dots, benefiting from the rigid environment formed by the cross-linking of PEG. Afterglow emission was obtained in S-dots powder at room temperature with a lifetime of 200 ms. Different patterns were fabricated to demonstrate the feasibility of sulfur-based RTP materials for anticounterfeiting applications. The presented results report an undiscovered property of elemental sulfur powder and related nanomaterials, which provides a versatile component for the development and applications of RTP materials.

https://doi.org/10.1021/acsomega.2c04307
ACS Omega 2022, 7, 30582−30589

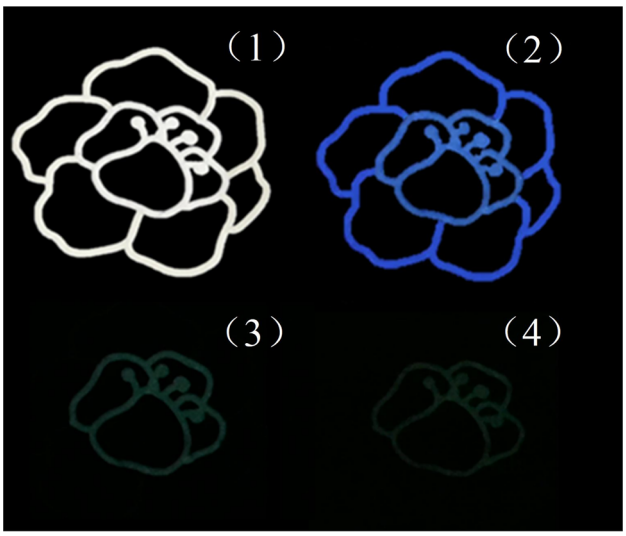

Figure 4. Photos of flower under (1) daylight, (2) under irradiation of 365 nm UV light, switching off excitation light for time intervals of (3) 0.05 and (4) 1 s.

MATERIALS AND METHODS

Materials. All the chemicals, including sulfur powder (99.9%), hydrogen peroxide (30%), polyethylene glycol (with different molecular weight), and sodium hydroxide were obtained from Aladdin. Sulfur powder, with a purity of 99.99% was obtained from Damas-beta.

Instrumentation. The UV-3600 spectrometer (Shimadzu, Japan) and F-7000 spectrometer (Hitachi, Japan) were used to record the UV−visible absorption spectra and fluorescence/phosphorescence spectra, respectively. The phosphorescence decay curves were recorded by an Edinburgh FLS-980 fluorescence spectrophotometer excited by a xenon arc lamp (Xe900) using the kinetic scan model. Temperature-dependent phosphorescence emission and excitation spectra were collected on a spectrometer of Horiba (FluoroMax+), with a delay time of 50 ms. Surface morphologies of the S-dots were characterized using a Tecnai G2 F20 high-resolution transmission electron microscope (HTEM) (FEI, USA) and a JPK atomic force microscope (AFM) (Bruker, Germany), respectively. Fourier-transformed infrared (FTIR) spectra were recorded on a Nicolet IS10 FTIR spectrometer (Thermo, USA). XPS spectra were recorded on an Escalab 250xi photoelectron spectrometer (Thermo, USA). The electron paramagnetic resonance (EPR) spectra were recorded on a Bruker A300 EPR Spectrometer.

Synthesis of S-dots. Sublimed sulfur powder (1.4 g), 50 mL of water, PEG-200 (3 mL), and sodium hydroxide (4 g), were added in order to a 100 mL round-bottom flask, and the mixture was allowed to react under continuous stirring at 90 °C for 72 h. Then, a different amount of H_2O_2 was added, and a strong blue emission appeared, indicating the formation of S-dots. Then, the as-obtained S-dots were freeze-dried to obtain the solid powder.

ASSOCIATED CONTENT

Supporting Information

The Supporting Information is available free of charge at https://pubs.acs.org/doi/10.1021/acsomega.2c04307.

Phosphorescence lifetimes and fractions of the emission intensity obtained from the fitting of experimental phosphorescence decay data under different conditions; content and weight percent of different elements; PL QY of S-dots powder under different excitation wavelengths; additional figures as described in the text (PDF)

Sulfur powder under 77 K (MP4)

S-Dots powder under room temperature (MP4)

AUTHOR INFORMATION

Corresponding Authors

Yu-e Shi − *Key Laboratory of Chemical Biology of Hebei Province Key Laboratory of Medicinal Chemistry and Molecular Diagnosis, Ministry of Education College of Chemistry & Environmental Science, Hebei University, Baoding 071002, China*; Email: shiyue1220@163.com

Zhenguang Wang − *Key Laboratory of Chemical Biology of Hebei Province Key Laboratory of Medicinal Chemistry and Molecular Diagnosis, Ministry of Education College of Chemistry & Environmental Science, Hebei University, Baoding 071002, China*; orcid.org/0000-0003-2001-5165; Email: zgwang@hbu.edu.cn

Ben Zhong Tang − *Department of Chemistry, Hong Kong Branch of Chinese National Engineering Research Center for Tissue Restoration and Reconstruction and Guangdong-Hong Kong-Macao Joint Laboratory of Optoelectronic and Magnetic Functional Materials, The Hong Kong University of Science and Technology, Kowloon, Hong Kong 999077, China; Shenzhen Institute of Aggregate Science and Technology, School of Science and Engineering, The Chinese University of Hong Kong, Shenzhen City, Guangdong 518172, China*; orcid.org/0000-0002-0293-964X; Email: tangbenz@cuhk.edu.cn

Authors

Jiaqi Guo − *Key Laboratory of Chemical Biology of Hebei Province Key Laboratory of Medicinal Chemistry and Molecular Diagnosis, Ministry of Education College of Chemistry & Environmental Science, Hebei University, Baoding 071002, China*

Zhangdi Lu − *Department of Chemistry, Hong Kong Branch of Chinese National Engineering Research Center for Tissue Restoration and Reconstruction and Guangdong-Hong Kong-Macao Joint Laboratory of Optoelectronic and Magnetic Functional Materials, The Hong Kong University of Science and Technology, Kowloon, Hong Kong 999077, China*

Chenmin Li − *Key Laboratory of Chemical Biology of Hebei Province Key Laboratory of Medicinal Chemistry and Molecular Diagnosis, Ministry of Education College of Chemistry & Environmental Science, Hebei University, Baoding 071002, China*

Yuming Miao − *Key Laboratory of Chemical Biology of Hebei Province Key Laboratory of Medicinal Chemistry and Molecular Diagnosis, Ministry of Education College of Chemistry & Environmental Science, Hebei University, Baoding 071002, China*

Bingbing Zhang − *Key Laboratory of Chemical Biology of Hebei Province Key Laboratory of Medicinal Chemistry and Molecular Diagnosis, Ministry of Education College of Chemistry & Environmental Science, Hebei University, Baoding 071002, China*

Jacky W. Y. Lam − *Department of Chemistry, Hong Kong Branch of Chinese National Engineering Research Center for Tissue Restoration and Reconstruction and Guangdong-Hong Kong-Macao Joint Laboratory of Optoelectronic and*

https://doi.org/10.1021/acsomega.2c04307
ACS Omega 2022, 7, 30582−30589

Magnetic Functional Materials, The Hong Kong University of Science and Technology, Kowloon, Hong Kong 999077, China

Complete contact information is available at: https://pubs.acs.org/10.1021/acsomega.2c04307

Author Contributions

#J.G. and Z.L. contributed equally.

Notes

The authors declare no competing financial interest.

■ ACKNOWLEDGMENTS

This work was financially supported by the National Natural Science Foundation of China (22175052), Science Fund for Creative Research Groups of Nature Science Foundation of Hebei Province(B2021201038), the Outstanding Youth Project of Natural Science Foundation of Hebei Province (B2020201060), One Hundred Talent Project of Hebei Province (E2019050011), Science and Technology Project of Hebei Education Department (BJ2020033), Natural Science Interdisciplinary Research Program of Hebei University (DXK201906), Research Innovation Team of College of Chemistry and Environmental Science of Hebei University (hxkytd-py2101), the Innovation and Technology Commission (ITC−CNERC14SC01), and the Natural Science Foundation of Guangdong Province (2019B121205002).

■ REFERENCES

(1) An, Z.; Zheng, C.; Tao, Y.; Chen, R.; Shi, H.; Chen, T.; Wang, Z.; Li, H.; Deng, R.; Liu, X.; Huang, W. Stabilizing triplet excited states for ultralong organic phosphorescence. *Nat. Mater.* **2015**, *14*, 685−690.

(2) Tian, Y.; Yang, J.; Liu, Z.; Gao, M.; Li, X.; Che, W.; Fang, M.; Li, Z. Multistage Stimulus-Responsive Room Temperature Phosphorescence Based on Host−Guest Doping Systems. *Angew. Chem., Int. Ed.* **2021**, *60*, 20259−20263.

(3) Zhou, B.; Yan, D. Simultaneous Long-Persistent Blue Luminescence and High Quantum Yield within 2D Organic−Metal Halide Perovskite Micro/Nanosheets. *Angew. Chem., Int. Ed.* **2019**, *58*, 15128−15135.

(4) Jiang, K.; Gao, X.; Feng, X.; Wang, Y.; Li, Z.; Lin, H. Carbon Dots with Dual-Emissive, Robust, and Aggregation-Induced Room-Temperature Phosphorescence Characteristics. *Angew. Chem., Int. Ed.* **2020**, *59*, 1263−1269.

(5) Ma, X.-K.; Liu, Y. Supramolecular Purely Organic Room-Temperature Phosphorescence. *Acc. Chem. Res.* **2021**, *54*, 3403−3414.

(6) Kirch, A.; Gmelch, M.; Reineke, S. Simultaneous Singlet−Singlet and Triplet−Singlet Förster Resonance Energy Transfer from a Single Donor Material. *J. Phys. Chem. Lett.* **2019**, *10*, 310−315.

(7) Zhao, W.; He, Z.; Tang, B. Z. Room-temperature phosphorescence from organic aggregates. *Nat. Rev. Mater.* **2020**, *5*, 869−885.

(8) Gao, H.; Ma, X. Recent progress on pure organic room temperature phosphorescent polymers. *Aggregate* **2021**, *2*, e38.

(9) Garain, S.; Kuila, S.; Garain, B. C.; Kataria, M.; Borah, A.; Pati, S. K.; George, S. J. Arylene Diimide Phosphors: Aggregation Modulated Twin Room Temperature Phosphorescence from Pyromellitic Diimides. *Angew. Chem., Int. Ed.* **2021**, *60*, 12323−12327.

(10) Peng, Q.; Ma, H.; Shuai, Z. Theory of Long-Lived Room-Temperature Phosphorescence in Organic Aggregates. *Acc. Chem. Res.* **2021**, *54*, 940−949.

(11) Singh, M.; Liu, K.; Qu, S.; Ma, H.; Shi, H.; An, Z.; Huang, W. Recent Advances of Cocrystals with Room Temperature Phosphorescence. *Adv. Opt. Mater.* **2021**, *9*, 2002197.

(12) Zhao, W.; He, Z.; Lam, J. W.Y.; Peng, Q.; Ma, H.; Shuai, Z.; Bai, G.; Hao, J.; Tang, B. Z. Rational Molecular Design for Achieving Persistent and Efficient Pure Organic Room-Temperature Phosphorescence. *Chem.* **2016**, *1*, 592−602.

(13) Kuila, S.; Garain, S.; Bandi, S.; George, S. J. All-Organic, Temporally Pure White Afterglow in Amorphous Films Using Complementary Blue and Greenish-Yellow Ultralong Room Temperature Phosphors. *Adv. Funct. Mater.* **2020**, *30*, 2003693.

(14) Wang, B.; Mu, Y.; Zhang, H.; Shi, H.; Chen, G.; Yu, Y.; Yang, Z.; Li, J.; Yu, J. Red Room-Temperature Phosphorescence of CDs@Zeolite Composites Triggered by Heteroatoms in Zeolite Frameworks. *ACS Cent. Sci.* **2019**, *5*, 349−356.

(15) Peng, C.; Chen, X.; Chen, M.; Lu, S.; Wang, Y.; Wu, S.; Liu, X.; Huang, W. Afterglow Carbon Dots: From Fundamentals to Applications. *Research* **2021**, *2021*, 6098925.

(16) Liu, Z.-Y.; Hu, J.-W.; Huang, C.-H.; Huang, T.-H.; Chen, D.-G.; Ho, S.-Y.; Chen, K.-Y.; Li, E. Y.; Chou, P.-T. Sulfur-Based Intramolecular Hydrogen-Bond: Excited-State Hydrogen-Bond On/Off Switch with Dual Room-Temperature Phosphorescence. *J. Am. Chem. Soc.* **2019**, *141*, 9885−9894.

(17) Wu, Z.; Nitsch, J.; Marder, T. B. Persistent Room-Temperature Phosphorescence from Purely Organic Molecules and Multi-Component Systems. *Adv. Opt. Mater.* **2021**, *9*, 2100411.

(18) Zhang, X.; Chen, X.; Guo, Y.; Gu, L.; Wu, Y.; Bindra, A. K.; Teo, W. L.; Wu, F.-G.; Zhao, Y. Thiolate-Assisted Route for Constructing Chalcogen Quantum Dots with Photoinduced Fluorescence Enhancement. *ACS Appl. Mater. Interfaces* **2021**, *13*, 48449−48456.

(19) Wang, B.; Lu, S. The light of carbon dots: From mechanism to applications. *Matter* **2022**, *5*, 110−149.

(20) Sun, Y.; Liu, S.; Sun, L.; Wu, S.; Hu, G.; Pang, X.; Smith, A. T.; Hu, C.; Zeng, S.; Wang, W.; Liu, Y.; Zheng, M. Ultralong lifetime and efficient room temperature phosphorescent carbon dots through multi-confinement structure design. *Nat. Commun.* **2020**, *11*, 5591.

(21) Jiang, K.; Wang, Y.; Cai, C.; Lin, H. Conversion of Carbon Dots from Fluorescence to Ultralong Room-Temperature Phosphorescence by Heating for Security Applications. *Adv. Mater.* **2018**, *30*, 1800783.

(22) Mukherjee, S.; Thilagar, P. Recent advances in purely organic phosphorescent materials. *Chem. Commun.* **2015**, *51*, 10988−11003.

(23) Boyd, D. A. Sulfur and Its Role In Modern Materials Science. *Angew. Chem., Int. Ed.* **2016**, *55*, 15486−15502.

(24) Kamyshny, A.; Borkenstein, C. G.; Ferdelman, T. G. Protocol for Quantitative Detection of Elemental Sulfur and Polysulfide Zero-Valent Sulfur Distribution in Natural Aquatic Samples. Geostand. *Geoanal. Res.* **2009**, *33*, 415−435.

(25) Wang, Y.; Zhao, Y.; Wu, J.; Li, M.; Tan, J.; Fu, W.; Tang, H.; Zhang, P. Negatively Charged Sulfur Quantum Dots for Treatment of Drug-Resistant Pathogenic Bacterial Infections. *Nano Lett.* **2021**, *21*, 9433−9441.

(26) Libenson, L.; Hadley, F. P.; McIlroy, A. P.; Wetzel, V. M.; Mellon, R. R. Antibacterial Effect of Elemental Sulfur. *J. Infect. Dis.* **1953**, *93*, 28−35.

(27) Sunil, K. S.; Bramhaiah, K.; Mandal, S.; Kar, S.; John, N. S.; Bhattacharyya, S. Emergence of Long Afterglow and Room Temperature Phosphorescence Emissions from Ultra-Small Sulfur Dots. *Mater. Adv.* **2022**, *3*, 2037−2046.

(28) Liu, G.; Niu, P.; Yin, L.; Cheng, H.-M. α-Sulfur Crystals as a Visible-Light-Active Photocatalyst. *J. Am. Chem. Soc.* **2012**, *134*, 9070−9073.

(29) Shi, Y.-e.; Zhang, P.; Yang, D.; Wang, Z. Synthesis, photoluminescence properties and sensing applications of luminescent sulfur nanodots. *Chem. Commun.* **2020**, *51*, 10982−10988.

(30) Shen, L.; Wang, H.; Liu, S.; Bai, Z.; Zhang, S.; Zhang, X.; Zhang, C. Assembling of Sulfur Quantum Dots in Fission of Sublimed Sulfur. *J. Am. Chem. Soc.* **2018**, *140*, 7878−7884.

(31) Wang, H.; Wang, Z.; Xiong, Y.; Kershaw, S. V.; Li, T.; Wang, Y.; Zhai, Y.; Rogach, A. L. Hydrogen Peroxide Assisted Synthesis of Highly Luminescent Sulfur Quantum Dots. *Angew. Chem., Int. Ed.* **2019**, *58*, 7040−7044.

(32) Song, Y.; Tan, J.; Wang, G.; Gao, P.; Lei, J.; Zhou, L. Oxygen accelerated scalable synthesis of highly fluorescent sulfur quantum dots. *Chem. Sci.* **2020**, *11*, 772−777.
(33) Chen, X.; Shen, S.; Guo, L.; Mao, S. S. Semiconductor-based Photocatalytic Hydrogen Generation. *Chem. Rev.* **2010**, *110*, 6503−6570.
(34) Moon, J.; Kalb, P. D.; Milian, L.; Northrup, P. A. Characterization of a sustainable sulfur polymer concrete using activated fillers. *Cem. Concr. Compos.* **2016**, *67*, 20−29.
(35) Toledo, J. R.; de Jesus, D. B.; Kianinia, M.; Leal, A. S.; Fantini, C.; Cury, L. A.; Sáfar, G. A. M.; Aharonovich, I.; Krambrock, K. Electron paramagnetic resonance signature of point defects in neutron-irradiated hexagonal boron nitride. *Phys. Rev. B* **2018**, *98*, 155203.
(36) Abass, A. K.; Ahmad, N. H. Indirect band gap investigation of orthorhombic single crystals of sulfur. *J. Phys. Chem. Solids* **1986**, *47*, 143−145.
(37) Hassanzadeh, P.; Andrews, L. Vibronic absorption spectra of sulfur (S3 and S4) in solid argon. *J. Phys. Chem.* **1992**, *96*, 6579−6585.
(38) Eckert, B.; Steudel, R. Molecular Spectra of Sulfur Molecules and Solid Sulfur Allotropes. In *Elemental Sulfur und Sulfur-Rich Compounds II*; Steudel, R., Ed.; Springer Berlin Heidelberg: Berlin, Heidelberg, 2003; pp 31−98.

https://doi.org/10.1021/acsomega.2c04307
ACS Omega 2022, 7, 30582−30589